



Article

Sea-Surface Small Target Detection Based on Four Features Extracted by FAST Algorithm

Di Zhao ^{1,2} , Hongyan Xing ^{1,2,*} , Haifeng Wang ^{1,2}, Huaizhou Zhang ^{1,2}, Xinyi Liang ^{1,2} and Haoqi Li ^{1,2}

¹ School of Electronic and Information Engineering, Nanjing University of Information Science and Technology, Nanjing 210044, China

² Jiangsu Key Laboratory of Meteorological Detection and Information Processing, Nanjing University of Information Science and Technology, Nanjing 210044, China

* Correspondence: xinghy@nuist.edu.cn

Abstract: On account of current algorithm and parameter design difficulties and low detection accuracy in feature extractions of small target detections in sea clutter environment, this paper proposes a correspondingly improved four feature extraction method by FAST. After the short-time Fourier transform is applied, a time–frequency distribution spectrogram of original data is generated. Candidate feature points (CFP) are first extracted by FAST algorithm, and then a four-feature extraction is implemented with FAST and DBSCAN combined. The feature distinction is enhanced through a feature optimization. Upon the construction of the four-dimensional feature vectors, XGBoost classifier algorithm classifies and detects these feature vectors. The genetic algorithm optimizes the hyperparameters in XGBoost and updates the decision threshold in real time to control the detection method’s false alarm rate. The IPIX dataset is employed for experimental verification. Verification results confirm that this proposed detection method has better performance than several other currently used detection methods. The detection performance is improved by 7% and 13.8% when observation time is set at 0.512 s and 1.024 s, respectively.

Keywords: sea clutter; target detection; feature extraction; FAST algorithm



Citation: Zhao, D.; Xing, H.; Wang, H.; Zhang, H.; Liang, X.; Li, H. Sea-Surface Small Target Detection Based on Four Features Extracted by FAST Algorithm. *J. Mar. Sci. Eng.* **2023**, *11*, 339. <https://doi.org/10.3390/jmse11020339>

Academic Editor: Wansuo Duan

Received: 3 January 2023

Revised: 18 January 2023

Accepted: 24 January 2023

Published: 3 February 2023



Copyright: © 2023 by the authors. Licensee MDPI, Basel, Switzerland. This article is an open access article distributed under the terms and conditions of the Creative Commons Attribution (CC BY) license (<https://creativecommons.org/licenses/by/4.0/>).

1. Introduction

Small floating target detections on the sea surface [1] remain a hotspot in radar detection at home and abroad. As backscattered radar signal returns from the sea surface, sea clutter has complex characteristics such as non-uniform, non-Gaussian, non-stationary, etc. Small floating targets such as boats, frogmen, and buoys are often hidden in sea clutter and difficult to detect because of their small radar cross-section (RCS) and weak radar returns. For those traditional detection methods based on general statistical characteristics or radar returns’ energy, it is hard to maintain high detection accuracy and low false alarm rate [2]. Accordingly, various obstacles exist in current detection technology.

At present, various feature extraction-based detection methods are proposed, including three categories. The first category is fractal characteristics-based detection method. From a non-energy perspective, fractal-based methods detect sea clutter and mine the data fractal features [3–5]. Haykin et al. uses fractal dimension characteristics of sea clutter to detect small floating targets in the earlier time [6]. Subsequently, the differences between sea clutter and target returns are also used for detection in terms of their single-scale fractal dimension features [7]. However, the fractal feature is single-dimensioned and requires a long observation time. Later on, detection methods to extract multifractal parameters are gradually developed. The second category is time–frequency (TF)-based detection methods. Based on signal TF information, TF-based methods map the original data to the TF distribution spaces, and then extract relevant features [8–11]. TF method is thus widely used in the sea clutter field effective for non-linear and non-stationary complex signals. Shui et al. constructs a three-feature detector which selects relative amplitude

features from the time domain, relative Doppler peak height and relative vector entropy features from the frequency domain [12]. As an improvement to [12], three TF features are re-extracted, which greatly improves their detection performances [13]. The third category is machine learning (ML) algorithm-based detection methods. ML algorithms such as the traditional support vector machine (SVM) and long-short term memory (LSTM) have been verified to be able to efficiently process data [14,15]. As deep learning-based detection methods adaptively extract multi-dimensional signal features through neural networks and exploit deeper information of the mined signals, a convolutional neural network is adopted to realize the sea clutter and noise classification, and to carry out a refined sea clutter suppression [16]. Since a neural network is a non-linear training process, extracted features display better discrimination and generalization. In addition, there are other target detection methods based on feature extraction. The graph connectivity density is calculated in [17,18], and whether the signal contains a target is judged by this single feature. Energy information is also frequently used as a feature in target detection. Shi et al. employs empirical mode decomposition (EMD) in [19] to decompose the signal into multiple intrinsic mode function (IMF) components, and the target existence is judged by the proportion of IMF components in the original signal energy. Utilizing a single feature for detection, though different from each other, these methods naturally miss some key representations in target signal detection.

In order to extract features more effectively, the one-dimensional time series are transformed into a two-dimensional matrix in different ways. This matrix must contain a strong mapping relationship with the original signal. As a case in point, the covariance matrix well reflects the correlation of the time series, statistics are constructed according to the eigenvalues of the covariance matrix and the statistical distribution is tested for an effective target detection [20]. Another dimension transformation method, the Gramian Angular Field (GAF), introduces a penalty inner product, which better suppresses Gaussian noise [21]. In addition, the TFD spectrogram generated by short-time Fourier transform (STFT) is also regarded as a two-dimensional image presented under dimension transformation. As the embodiment of signal energy, the spectrogram effectively indicates signal characteristics due to its non-negativity and good suppression of cross-terms [22,23].

Due to the dimension transformation processing of the original time series, some image processing methods are adopted for their convenience and efficiency in recent years. Different from image matching, the key to distinguish sea clutter from target returns is matching points' amplitude and gratitude information, while the specific position information is discarded. A symmetric positive definite (SPD) matrix of Riemannian manifold is introduced to map the 2D spectrogram to the Riemann space in [24]. The SIFT descriptor is then used to extract 128 dimensional features containing gradient information, while the domain of sea clutter and target returns is divided by calculating the Riemann distance. However, an ensuing problem of increased calculation time emerges. The cumbersome calculation workload calls for a network simplification. Because Features from Accelerated Segment Test (FAST) algorithm excels for its convenience and speed, this paper uses FAST to extract the necessary multi-dimensional features.

The following is the general flow of the proposed method. This paper performs short-time Fourier transform (STFT) on the original data and generates a TF distribution spectrogram. Four features are then extracted in sequence in this research. It uses FAST to extract the candidate feature points in the TF distribution spectrogram as the first overall feature. The second feature is obtained by computing the average distributed energy of all CFPs. Density-Based Spatial Clustering of Applications with Noise (DBSCAN) algorithm is used to divide clusters to constitute the third feature. Finally, the cluster with the largest number of CFPs is selected, and the number of CFP is used as the fourth feature. In order to reduce the impact of abnormal CFPs on the feature distinguishability and standardize the process, the resulted four features are optimized first, followed by a normalization process, and a four-dimensional feature space is accordingly constructed. What follows in this paper is the use of the XGBoost algorithm as the classifier, and the introduction of

the genetic algorithm to optimize the hyperparameter group in XGBoost. The judgment threshold is updated in real time, according to the predicted value output by XGBoost, so as to realize a controllable false alarm rate of the detection method. A detection method based on four FAST-induced features is proposed, and the IPIX dataset is used to verify the advantage and stability in the detection performance of the proposed method.

2. Theoretical Basis of Feature Extraction

The first thing to consider in feature extraction-based target detection is actually the issue of combining general features into feature vectors and a reasonable division of the vector spaces. The target detection problem thus undergoes a transformation. Based on an effective characterization of data energy information by the spectrogram and an excellent performance of FAST algorithm for CFPs, four features are extracted and optimized in this paper. There is a detailed description concerning the transformation, feature extraction and optimization.

2.1. Target Detection Problem Transformation

It is assumed that N consecutive pulses received by the radar constitute the original observation data $s = [s(1), s(2), \dots, s(N)]^T$. In this way, a small target detection problem on the sea surface is transformed into a hypothesis testing issue:

$$\begin{cases} H_0 : s = c \\ H_1 : s = e + c \end{cases} \quad (1)$$

where e is the target returns and c is the pure sea clutter. When the original observation data contain only pure sea clutter, i.e., there is no observation target, it is judged as H_0 hypothesis. When the original observation data contain target returns, i.e., there may be an observation target here, it is judged as H_1 hypothesis. Thus, the target detection problem is transformed into a binary classification. The design focus of the feature extraction detection is to improve the distinction between different features, divide feature vectors into different domains, and set decision thresholds.

2.2. Short-Time Fourier Transform

Due to the complex characteristics of sea clutter, it is hard to achieve high detection accuracy with a multi-dimensional feature extraction from a single domain. As an improvement, on the basis of Fourier transform, the short-time Fourier transform (STFT) then introduces the window function, which offers a limited support in the time–frequency domain. Therefore, STFT is used to realize the time–frequency signal positioning. At the same time, STFT has a strong anti-interference, and a strong capability of processing frequency-domain diversity signals, while it does not generate cross-interference terms. STFT is used to transform the original signals into a time–frequency distribution matrix, whose formula is

$$STFT(t, \omega) = \int_{-\infty}^{+\infty} s(\tau)h * (\tau - t)e^{-j\omega\tau}d\tau. \quad (2)$$

A modulo operation on the time–frequency distribution matrix is performed to obtain a time–frequency distribution spectrogram

$$SPEC(t, \omega) = \|STFT(t, \omega)\|. \quad (3)$$

A time–frequency distribution spectrogram is obtained by (3). The spectrogram has constant positivity and contains all real numbers. Since any window function satisfies $\|h(\tau)\| = 1$, it can be inferred that

$$\iint SPEC_x(t, \omega)dtd\Omega = E_x. \quad (4)$$

It is clear from (4) that the spectrogram is actually a signal energy distribution. Converting the original signal into a time–frequency distribution spectrogram effectively provides the signal energy information. The time–frequency distribution spectrogram is rasterized, where the spectrogram is divided into n points and l points from the horizontal and vertical directions, respectively corresponding to the time domain axis and frequency domain axis of the spectrogram. Therefore, $SPEC(t, \omega)$ is converted into $SPEC(n, l)$, correspondingly. Next, the spectrogram is normalized, and its normalization formula is defined as

$$NSPEC(n, l) = \frac{SPEC(n, l) - \mu(n, l)}{\sigma(n, l)}. \tag{5}$$

The normalization process means that when the detection signal is pure sea clutter time series, it is a random process with zero mean and unit variance in the normalized spectrogram. By contrast, when the detection signal contains the target returns, there are obvious relevant differences between this signal and the normalized spectrogram of pure sea clutter [10]. The formulas for the mean function $\mu(n, l)$ and the standard deviation function $\sigma(n, l)$ are as follows:

$$\mu(n, l) = \frac{1}{n \times l} \sum_{n=1}^N \sum_{l=1}^L SPEC(n, l), \tag{6}$$

$$\sigma(n, l) = \sqrt{\frac{1}{n \times l - 1} \sum_{n=1}^N \sum_{l=1}^L (SPEC(n, l) - \mu(n, l))^2}. \tag{7}$$

2.3. Feature Extraction Based on FAST Algorithm

Due to the non-uniform, non-Gaussian and non-stationary characteristics of sea clutter, it is difficult to reconstruct complex sea clutter signals with simple mathematical models. Therefore, it is difficult to achieve optimum detection results with traditional single-feature based detection methods. After generating the time–frequency distribution spectrogram, the FAST algorithm is used to extract four features in the spectrogram. Specific extraction methods of the four features are given below.

As a feature point detection algorithm [25,26], FAST selects a 7×7 square space in the image and draws a circle in this square at its center point with a radius of 3.4. FAST, then, respectively, compares the pixel values of the center point and 16 points that the circle passes. This is followed by a pixel value subtraction by the center point to the above-mentioned 16 points. Among the subtraction differences, if there are more than 12 values greater than the set threshold ths , the center point is considered as a candidate feature point (CFP). When FAST algorithm is introduced for feature extraction, the time–frequency distribution spectrogram converted from the original signal becomes the image to be further extracted. The energy value corresponding to each point in the spectrogram becomes the pixel value to be compared in the FAST algorithm. The CFPs extracted by the FAST algorithm are considered as the edge points of their respective energy peaks. The feature points detected by FAST algorithm contain only location information and are still unfit for direct target detection effectively [27]. This paper counts the following feature values including the number of CFPs, energy quantities, the number of clusters obtained and the number of CFPs in the largest cluster:

- ζ_1 : the number of CFPs in the time–frequency distribution spectrogram;
- ζ_2 : average distribution energy quantity of CFPs;
- ζ_3 : the number of clusters obtained by clustering CFPs;
- ζ_4 : the number of CFPs in the largest cluster.

Among them, ζ_1 is directly obtained by the FAST algorithm to count the CFPs. ζ_2 is calculated from ζ_1 in the original spectrogram. DBSCAN algorithm is used to calculate ζ_3 .

ζ_4 is obtained by selecting the cluster with the largest CFP number among all the clusters in ζ_3 , and then taking the number of CFPs in this newly obtained cluster as its value.

Here is a brief description of the clustering algorithm. Density-Based Spatial Clustering of Applications with Noise (DBSCAN) is an unsupervised ML clustering algorithm [28]. It is necessary to first manually set its two key parameters. One parameter is the maximum scanning radius r_{max} , while the other is the minimum number of included points Pt_{min} . A point is regarded as a core point if there are more than or equal to Pt_{min} points within the radius r_{max} of this point. A point is regarded as a boundary point if it is not a core point and is located in the radius r_{max} of a core point. A point is regarded as a noise point if it is not located in the radius r_{max} of any core point. The calculation now begins with r_{max} and Pt_{min} manual setting, and then a random CFP selection. All corresponding core points and boundary points are aggregated into the same cluster, and the noise points are removed.

A CFP picking is obligatory since the energy quantity of some CFPs may be too high or too low with primary CFP extraction, resulting in a serious impact on ζ_2 , and thus the final detection accuracy. All the CFPs are arranged in ascending order of energy, and then the first one-eighth and the last one-eighth of the CFPs are removed, which eliminates the influence of abnormal CFPs and optimizes each feature. Then, the four features are normalized, for different features have different value ranges. Therefore, for the i -th feature and the obtained P four-feature samples, the calculation formula is as follows:

$$\bar{\zeta}_i = \frac{\zeta_i - \frac{1}{P} \sum_{p=1}^P \zeta_i(p)}{\sqrt{\frac{1}{P-1} \sum_{p=1}^P (\zeta_i(p) - \frac{1}{P} \sum_{p=1}^P \zeta_i(p))^2}}, i = 1, 2, 3, 4. \tag{8}$$

A four-dimensional feature space is constructed taking each feature as a dimension, thereby a four-dimensional space vector is obtained as

$$\bar{\zeta} = [\bar{\zeta}_1, \bar{\zeta}_2, \bar{\zeta}_3, \bar{\zeta}_4]^T. \tag{9}$$

The obtained four-dimensional vector effectively reflects the difference between the pure sea clutter and the target returns in the time–frequency distribution, which is beneficial to the subsequent target detection process.

3. Small Target Detection on Sea Surface Based on Four FAST Features

A confusion matrix is usually used to judge feature extraction-based target detection method. The detection probability and the false alarm rate are commonly used parameters. The detection probability is the proportion of correctly judged samples among all actually targeted samples. The false alarm rate is the proportion of wrongly judged samples among all actually untargeted samples. A false alarm rate increase will lead to the network judgment imbalance, and it needs to be considered to control the false alarm rate continuously. The target detection requirement for the false alarm rate is no more than 10^{-3} . Since the detection probability and the false alarm rate are calculated based on the same confusion matrix, they are mutually checked and balanced. A lower false alarm rate results in a lower detection probability. Therefore, the classifier’s detection probability with a constant low false alarm rate is the criterion for judging the classifier’s target detection effect.

In order to realize data classification and detection of sea cluster and target returns as well as real-time false alarm controllability, this XGBoost classifier is optimized first to make up for its previous inadequacy as illustrated in relevant studies. Then, optimized XGBoost algorithm classifies the extracted four-dimensional feature vectors. So far, combining the FAST-based feature extraction with the optimized XGBoost classifier, this paper proposes a FAST four-feature based small target detection method on the sea surface and elaborates the detection results.

3.1. XGBoost Classifier

Most of the currently adopted methods, such as support vector machine (SVM) [29], linear regression (LR) [30], and decision tree (DT) [31], are implemented for a binary classification, but they are unable to guarantee fairly accurate detection results for uncontrollable false alarms. Therefore, this paper chooses the XGBoost algorithm to construct the classifier, which is a multi-class regression tree ensemble algorithm combining multiple different decision tree models into a relatively better model [32]. The model formula is

$$\hat{y}_i^{(t)} = \sum_{k=1}^t f_k(x_i) = \hat{y}_i^{(t-1)} + f_t(x_i), \tag{10}$$

where $\hat{y}_i^{(t)}$ is the predicted value of the model for samples after t iterations, t is the total number of trees. f_k is a function in the function space F , x_i is the i -th sample of the input data, $\hat{y}_i^{(t-1)}$ is the prediction result of the first $t-1$ trees, and $f_t(x_i)$ is the model of the t -th tree. Since XGBoost adopts a gradient boosting strategy, each new decision tree added in the training process gradually fits the previous total learning error, thus ensuring a better training effect. The objective function of the XGBoost algorithm is

$$Obj^{(t)} = l(y_i, \hat{y}_i^{(t-1)} + f_t(x_i)) + \Omega(f_t) + C, \tag{11}$$

where l is the loss function, y_i is the real sample value, $\Omega(f_t)$ is the regular term calculated by all decision trees, and C is a constant. One of XGBoost advantages lies in its expansion of the objective function with a second-order Taylor function, which is

$$Obj^{(t)} = \sum_{i=1}^n [l(y_i, \hat{y}_i^{(t-1)}) + g_i f_t(x_i) + \frac{1}{2} h_i f_t^2(x_i)] + \Omega(f_t) + C, \tag{12}$$

where g_i and h_i are the first derivative and the second derivative after expansion, respectively. All the samples x_i of the j -th leaf node are classified into the sample set of a leaf node, defined as $I_j = \{i | q(x_i) = j\}$; then, formula (12) is rewritten as

$$Obj^{(t)} = \sum_{j=1}^T [(\sum_{i \in I_j} g_i) w_j + \frac{1}{2} (\sum_{i \in I_j} h_i + \lambda) w_j^2] + \beta T. \tag{13}$$

Among these, β is the influence coefficient, λ is the L_2 regularization coefficient, T is the number of leaf nodes of the current tree, and w_j is the weight value of the leaf node. Let the derivative of the objective function be zero; the optimal weight is obtained, and the final objective function is

$$Obj = -\frac{1}{2} \sum_{j=1}^T \frac{(\sum_{i \in I_j} g_i)^2}{\sum_{i \in I_j} h_i + \lambda} + \beta T, \tag{14}$$

where the tree construction plays a key role. The parameters of a decision tree are called hyperparameters. The hyperparameter optimization process and the controllable implementation method of false alarms are described in detail below.

3.2. XGBoost Hyperparameter Optimization and False Alarm Rate Controlling

The training results of the XGBoost algorithm are affected by the hyperparameters in the model. Table 1 shows some of XGBoost hyperparameters and their default values. An improper selection of hyperparameter values seriously affects detection results and then detection accuracies. Therefore, genetic algorithm (GA) is used to first optimize the four hyperparameters listed in Table 1 [33]. A total of 50 randomly generated hyperparameter groups are set, and the values of all hyperparameter groups are converted into binary codes.

After group selection, crossover, mutation and elimination, a new hyperparameter group value is obtained, and the detection probability is used as a GA fitness function. After the above multiple iteration, it is taken as the condition for the iteration termination whether the difference between the highest and lowest fitness value is less than 10^{-5} . Finally, the original model obtains the optimal hyperparameter group and an optimized XGBoost model most suitable for the training samples.

Table 1. Descriptions and default values of XGBoost hyperparameters.

Hyperparameter Name	Meaning	Defaults
learning_rate	Learning Rate of the Network	0.3
max_depth	Maximum Depth of Tree	6
min_child_weight	Minimum Sum of Instance Weights in Subsets	1
subsample	Instance Subsample Ratio	1

After training with this optimized XGBoost model, the predicted value ρ corresponding to each group of four-dimensional feature vectors is obtained. In order to realize the false alarm controllability, all predicted values that are actually sea clutter samples are picked up, denoted as $\rho_0, \rho_1, \dots, \rho_{n-1}$. When the false alarm rate is set, the decision threshold γ is calculated:

$$\gamma = \rho_{\lfloor P_{fa} \times n \rfloor} \tag{15}$$

Then, it compares all the predicted values with the decision threshold. If $\rho < \gamma$, it is judged not to contain the target echo and it belongs to H_0 hypothesis. If $\rho > \gamma$, it is judged as to contain the target echo and it belongs to H_1 hypothesis. The detection probability is calculated according to the judgment results, with a controlled false alarm rate [34,35]. In GA iterative process, the prediction values obtained from each group training with different hyperparameters are calculated according to (15) to update the decision threshold, so as to effectively realize a real-time control of the false alarm rate.

3.3. Detection Method Based on Four FAST Features

Combining the FAST-based feature extraction with the optimized XGBoost classifier, the FAST four-feature (FAST-4F) detection method is proposed. The flowchart is illustrated in Figure 1. First, the IPIX dataset is used as original data, whose detailed description is given below in Period 4. The original data are converted into a TF distribution spectrogram using the STFT, and then the TF distribution spectrogram is normalized. The FAST algorithm extracts CFPs in the spectrogram and the CFPs are counted as ξ_1 , which is used to calculate ξ_2 . DBSCAN is used to divide clusters and count them as ξ_3 , which finally results in ξ_4 . Next, the four features are further normalized and unified, so as to construct a four-dimensional feature vector. So far, the feature extraction finishes.

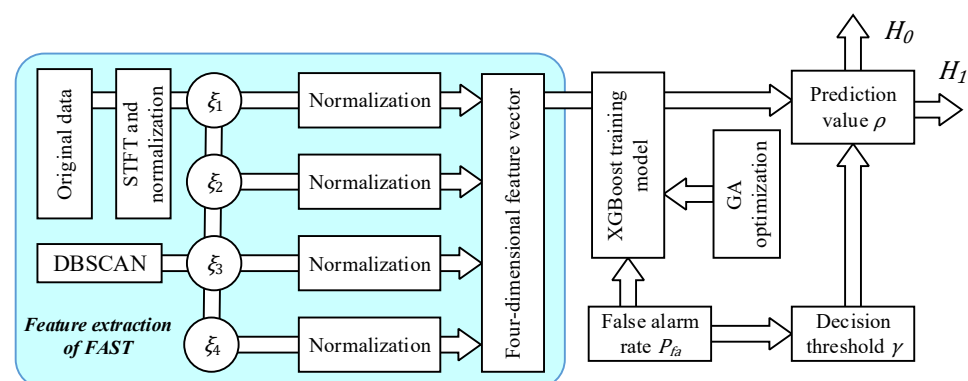


Figure 1. Flowchart of the FAST-4F detection method.

What follows is the classification detection procedure, where XGBoost training model is used to perform binary classification on the constructed four-dimensional feature vector. GA is used to optimize the hyperparameters in the XGBoost training model. The decision threshold γ is obtained by taking the false alarm rate P_{fa} into account. The prediction value ρ obtained by the XGBoost training model is compared with γ to obtain the final classification result.

4. Experiment and Performance Analysis

The data used in this paper originate from IPIX radar target database, which was collected on the east coast of Canada in 1993. This radar works in X-band and operates at a frequency of 9.39 GHz. The experiment required 10 sets of data. Each set of data consists of 14 adjacent cells. Each distance cell contains 131,072 pulses. The distance resolution is 30 m, and the target is a polystyrene foam ball wrapped with a wire mesh, approximately 1 m in diameter. According to different data transmission and reception modes, HH, HV, VH and VV polarizations are obtained. The cells that contain targets are regarded as primary cells, and the cells affected by targets are regarded as secondary cells. Table 2 shows the specific situation of IPIX radar data.

Table 2. Specific case description of IPIX radar data.

Data Name	Wind Speed (km/h)	Wave Height (m)	Angle (°)	Primary Cell	Secondary Cell
#17	9	2.2	9	9	8,10,11
#26	9	1.1	97	7	6,8
#30	19	0.9	98	7	6,8
#31	19	0.9	98	7	6,8,9
#40	9	1.0	88	7	5,6,8
#54	20	0.7	8	8	7,9,10
#280	10	1.6	180	8	7,9,10
#310	33	0.9	30	7	6,8,9
#311	33	0.9	40	7	6,8,9
#320	28	0.9	30	7	6,8,9

4.1. Parameter Selection at Different Polarizations

Due to differences in the time–frequency distribution spectrograms at different polarizations, the distributions of FAST-extracted CFPs are affected, which makes it difficult to manifest the differences between sea clutter and target returns. Therefore, various parameters in the detection method need to be adjusted for different polarizations. Through analysis, the parameters to be adjusted are selected, including the window length in STFT L_{window} , the overlapping length of adjacent windows in STFT $L_{noverlap}$, the threshold set in FAST ths , the maximum scanning radius in DBSCAN r_{max} and the minimum number of included points in DBSCAN $P_{t_{min}}$. Table 3 shows the final selection results of each parameter. Compared with HV and VH polarizations, the time–frequency distribution spectrograms at HH and VV polarizations are relatively smooth, so $L_{noverlap}$ is shortened to simplify the spectrogram, thereby reducing the calculation time and complexity. In addition, spectrograms at HV and VH polarizations are relatively rough, so DBSCAN parameters need to be adjusted to reduce cluster numbers. Through continuous testing, various parameters are adjusted properly, which effectively enhance differences between the characteristics of sea clutter data and that of target return data, and play a crucial role in the subsequent detection process.

Table 3. Setting values of various parameters at different polarizations.

Polarization Mode	L_{window}	$L_{noverlap}$	ths	r_{max}	Pt_{min}
HH	16	8	0.25	2	5
HV	16	15	0.27	3	3
VH	16	15	0.28	3	3
VV	16	8	0.35	2	5

4.2. Feature Feasibility and Visualization

To verify feature separability of sea clutter and target returns, the data of #54 at the HH polarization are selected for the experiment in the first hand. Cell 1 (sea clutter) and Cell 8 (target returns) of #54 data are selected. The observation time is set to 0.512 s, that is, each group of data contains 512 points. Two data cells are divided into 256 groups, with a total of 512 groups. Figure 2 shows CFP distributions selected by the fifth group of Cell 1 and Cell 8, respectively, with red dots being the selected CFPs. It is apparent from (a) and (b) that many CFPs are extracted from sea clutter with a relatively wider distribution, while few CFPs are extracted from target returns. This is because the spectrogram of sea clutter is rougher than that of target returns, the former of which may contain more peaks and aid in easier detection of CFPs. In addition, the CFPs extracted from sea clutter are more discrete, bringing about more clusters after DBSCAN than those of target returns. The largest cluster’s CFP number from sea clutter is also higher. Apparently, ζ_1 , ζ_3 and ζ_4 are somehow distinguished.

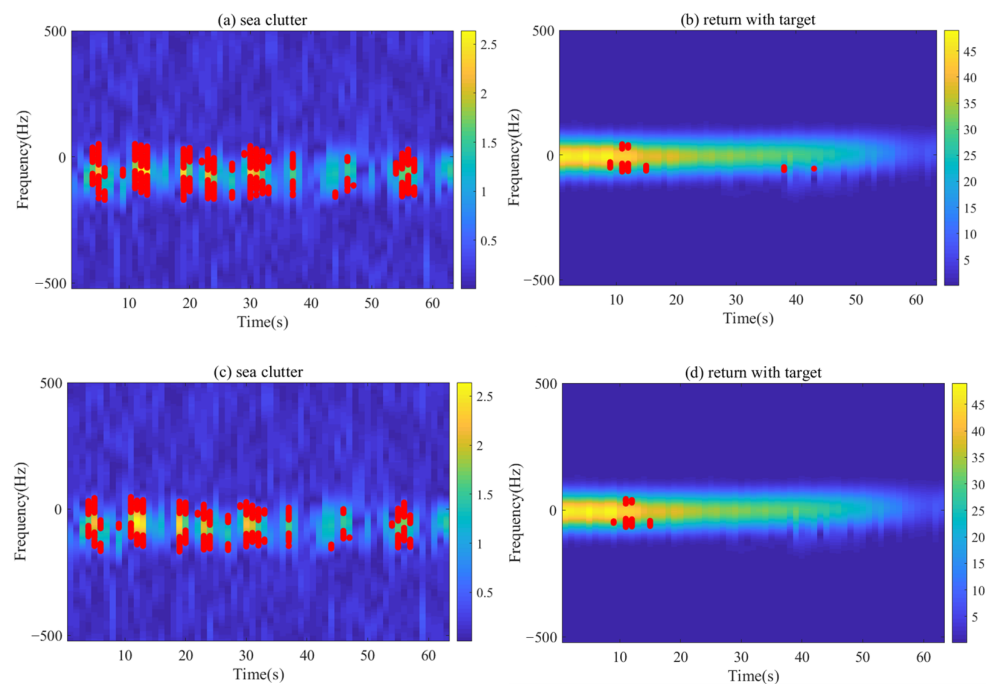


Figure 2. Distribution contrast of CFPs between sea clutter and target returns of #54 data at the HH polarization. (a) Spectrogram of sea clutter containing CFPs. (b) Spectrogram of target returns containing CFPs. (c) Spectrogram of sea clutter containing CFPs after optimization. (d) Spectrogram of target returns containing CFPs after optimization.

Then, a secondary picking to all CFPs is performed, removing the first and the last one-eighth of the CFPs after sequencing with the results listed in (c) and (d), respectively. There are only unobvious changes in (a) and (c), and some of their cluster areas in (c) even become slightly smaller. In (d), compared to the scattered CFPs on the right side of (b), it has been screened out in (d), while the main CFPs are gathered in the higher energy part on the left side, and the CFPs are more concentrated. Since differences are hardly noticeable for the

naked eye, all the required specific values of the four features are counted in Table 4. It can be determined that ζ_1 changes are relatively regular due to CFP statistics. Small ζ_3 changes are most probably caused by the removal of clusters that are formed by abnormal CFPs in the edge area. ζ_4 changes are relatively larger, because the spectrogram of target returns originally contains less CFPs, and the number of ζ_4 decreases sharply after picking, which is not the case in sea clutter. ζ_2 of sea clutter and target returns change in two directions. The ζ_2 of sea clutter is smaller and that of target returns is larger, which somehow widens ζ_2 gaps. For more complex spectrogram cases, abnormal CFPs are scattered loosely in the graph. Although this method sacrifices some CFPs, it better enhances the ζ_2 differences.

Table 4. Comparison of four features before and after optimization.

Optimization Situation	ζ_1	ζ_2	ζ_3	ζ_4
Sea clutter before optimization	1224	1.0896	62	262
Sea clutter after optimization	918	1.0424	61	219
Target returns before optimization	77	29.7358	6	12
Target returns after optimization	58	30.4369	5	6

Next, all four features of 512 sets of data are calculated and counted into a histogram, as shown in Figure 3. It is apparent from the figure that ζ_2 has the best separation effect, the overlap is the smallest, and ζ_2 of most sea clutter data is clustered below 8, which is convergent. ζ_1 and ζ_3 also have a good separation effect. However, there are many overlapping parts between ζ_4 of sea clutter and target returns. Therefore, the detection ability of ζ_1 , ζ_2 and ζ_3 is strong, and the detection ability of ζ_4 is relatively weak.

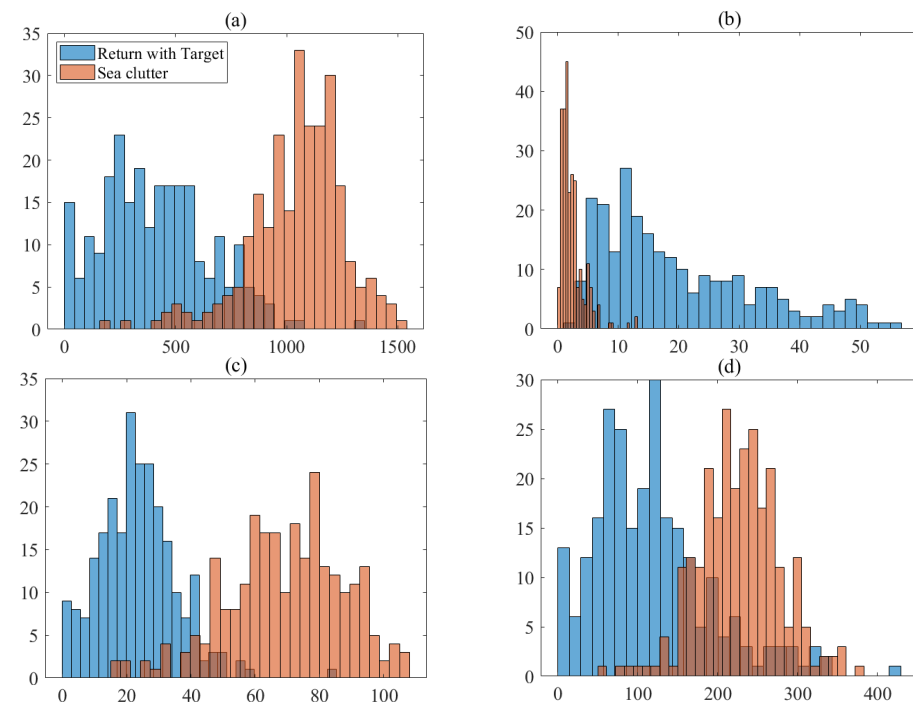


Figure 3. Histogram contrasts of the four features of sea clutter and target returns of #54 data at the HH polarization. (a) ζ_1 . (b) ζ_2 . (c) ζ_3 . (d) ζ_4 .

Below are the comparison results of #54 data at the HH polarization. For different data, the discrimination degree of the four features is also different. In order to verify this

point of view, a total of 512 sets of data from Cell 1 (sea clutter) and Cell 7 (target returns) of #320 data at the HH polarization are selected and tested, as shown in Figure 4. It illustrates that the separation effect of ζ_1 and ζ_2 becomes worse, while the separation effect of ζ_3 is the best at this time. Therefore, the four features contain a certain complementarity, which effectively enhances the generalization ability of the detection method.

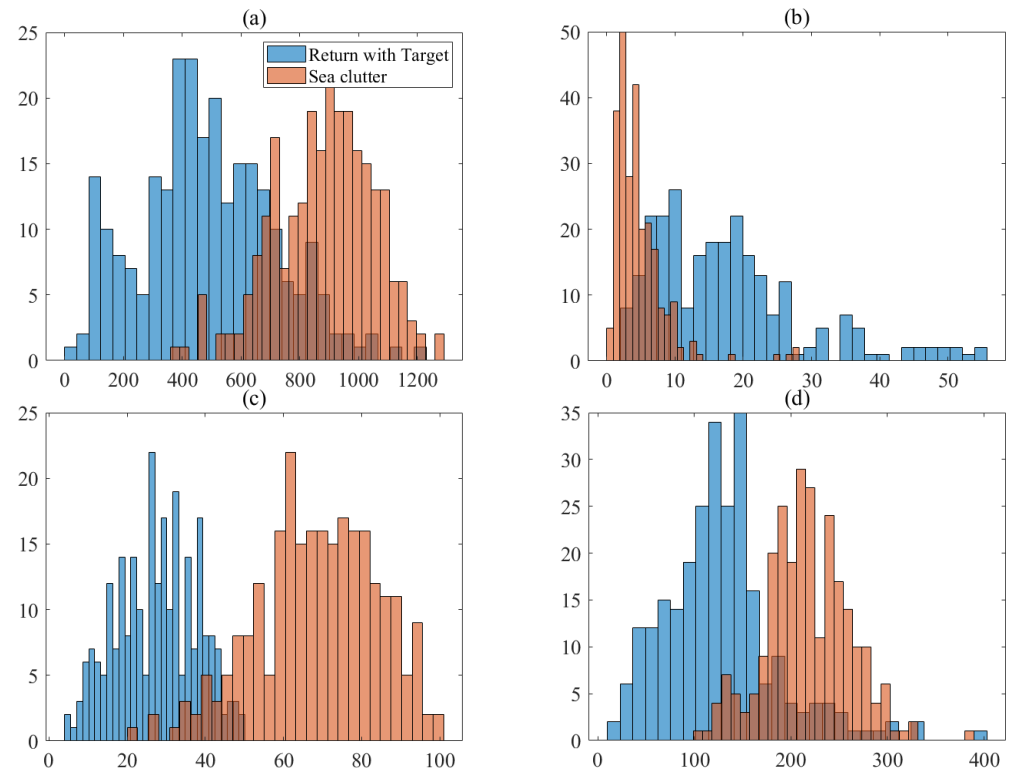


Figure 4. Histogram contrasts of the four features between sea clutter and target returns of #320 data at the HH polarization. (a) ζ_1 . (b) ζ_2 . (c) ζ_3 . (d) ζ_4 .

4.3. Detection Performance Comparison

In order to verify the detection performance of the proposed method, the selected data are independently tested at different polarizations. The false alarm rate is set at $P_{fa} = 10^{-3}$, and observation times are 0.512 s and 1.024 s, respectively. Figure 5 depicts contrasts of FAST-4F detection probabilities at four polarizations. Figure 5a illustrates that the FAST-4F has better detection results for #54, #311, and #320 data, and the detection probabilities of #54 data at HH and HV polarizations even reach 100%. In (b), most of the data display a dramatic improvement with an extended observation time. It confirms that this detection method has good detection performance. The overall detection effects at HV and VH polarizations are better than those at HH and VV polarizations, because the two cross-polarizations have higher average signal-to-clutter ratios (ASCR) than the two co-polarizations. At the same time, the VV polarization produces greater Bragg scattering than the HH polarization, resulting in a lower ASCR of VV than HH. The detection probability is significantly affected by ASCR, so the HV and VH polarizations have better detection results.

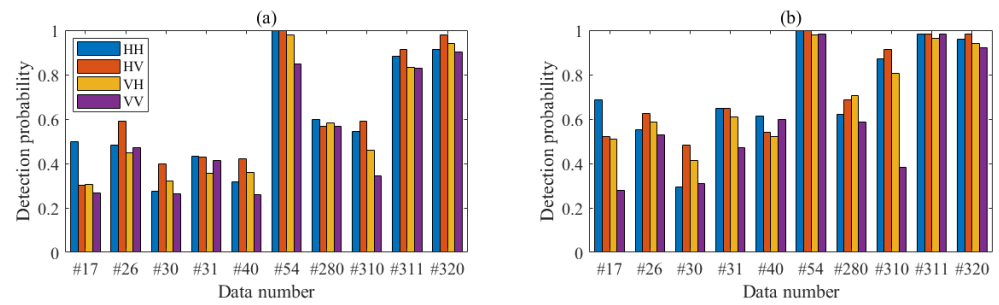


Figure 5. Detection probability contrasts of FAST four-feature detection at four polarizations, when (a) $N = 512$, (b) $N = 1024$ and $P_{fa} = 10^{-3}$.

Next, FAST-4F is compared with other detection methods to further verify its detection performance. Figure 6 shows the detection effect contrast between FAST-4F and other four detection methods at four polarizations. Other detection methods are Fourier transform, graph connectivity density (GCD) [18], tri-feature detector [12] and average energy ratio (AER), respectively [19]. It is apparent from Figure 6 that at HH and VV polarizations, FAST-4F has a fundamentally better detection probability than other detection methods do. The same is also true under HH and VV with a low ASCR. At HV and VH polarizations, FAST-4F may have a lower detection probability for some part of data, but its overall detection effect is still slightly better. Compared with the Fourier transform detection, FAST-4F uses the TF distribution, which effectively overcomes the problems that the time domain cannot be combined with the frequency domain, and that Fourier transform has some difficulty extracting features. Compared with those with fewer feature dimensions such as GCD, tri-feature detector and AER, FAST algorithm in FAST-4F extracts the four-dimensional feature vector, enhancing its generalization and calculation. FAST-4F is simple and straightforward, greatly reducing the computational complexity and design difficulty. The average detection probabilities with these four methods, namely Fourier transform, GCD, tri-feature detector, AER and FAST-4F are 17.01%, 38.02%, 51.23%, 52.33% and 56.03%, respectively. Compared with AER, FAST-4F still has an over 7% performance improvement. All of these figures clarify a fairly reliable and stable detection performance of FAST four-feature detection method.

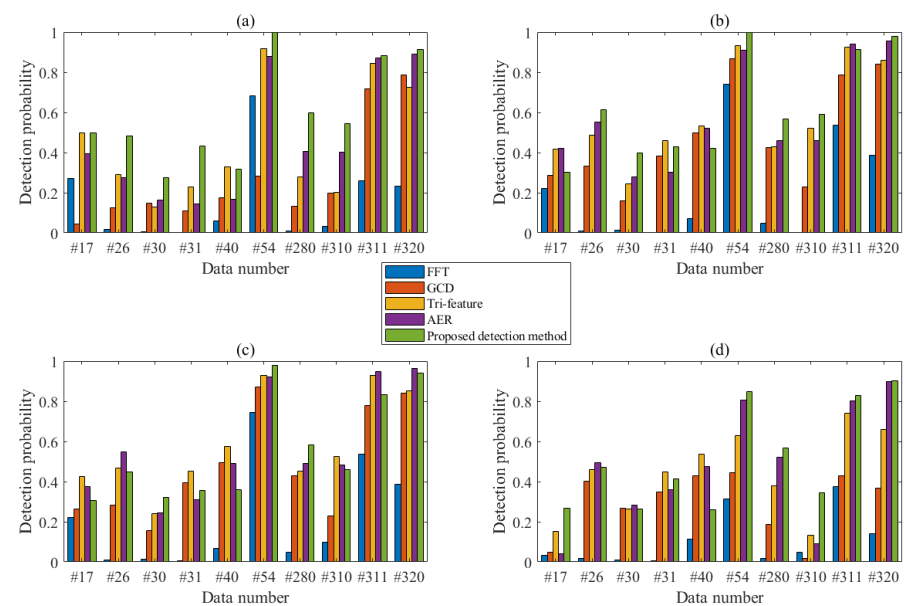


Figure 6. Contrasts of detection probabilities of five detection methods at (a) HH, (b) HV, (c) VH and (d) VV, when $N = 512$ and $P_{fa} = 10^{-3}$.

Next, the IPIX dataset is split into segments of length 1024, and the above five detection methods are compared again. As is shown in Figure 7, FAST-4F has an impressive detection improvement at HH and HV polarizations. Despite the fact that the detection at VH and VV polarizations is slightly worse than that of AER, it still has a general detection probability. The average detection probabilities of Fourier transform, GCD, tri-feature detector, AER and FAST-4F are 20.51%, 45.12%, 56.46%, 60.83% and 69.23%, respectively. In terms of observation time, compared with $N = 512$, FAST-4F detection is improved by 23.56%, when $N = 1024$. Therefore, an observation time extension significantly improves its detection probability. When compared with AER, FAST-4F detection is improved by 13.8%, a further improvement over previous detection performance. However, the detection effect at HV and VH polarizations is fairly worse, because the TFD spectrogram under cross-polarization is not smooth enough, with detection at the HH polarization always being better. Therefore, it is still necessary to improve the feature extraction parameters under the two cross-polarizations to make up for the TFD spectrogram shortcomings.

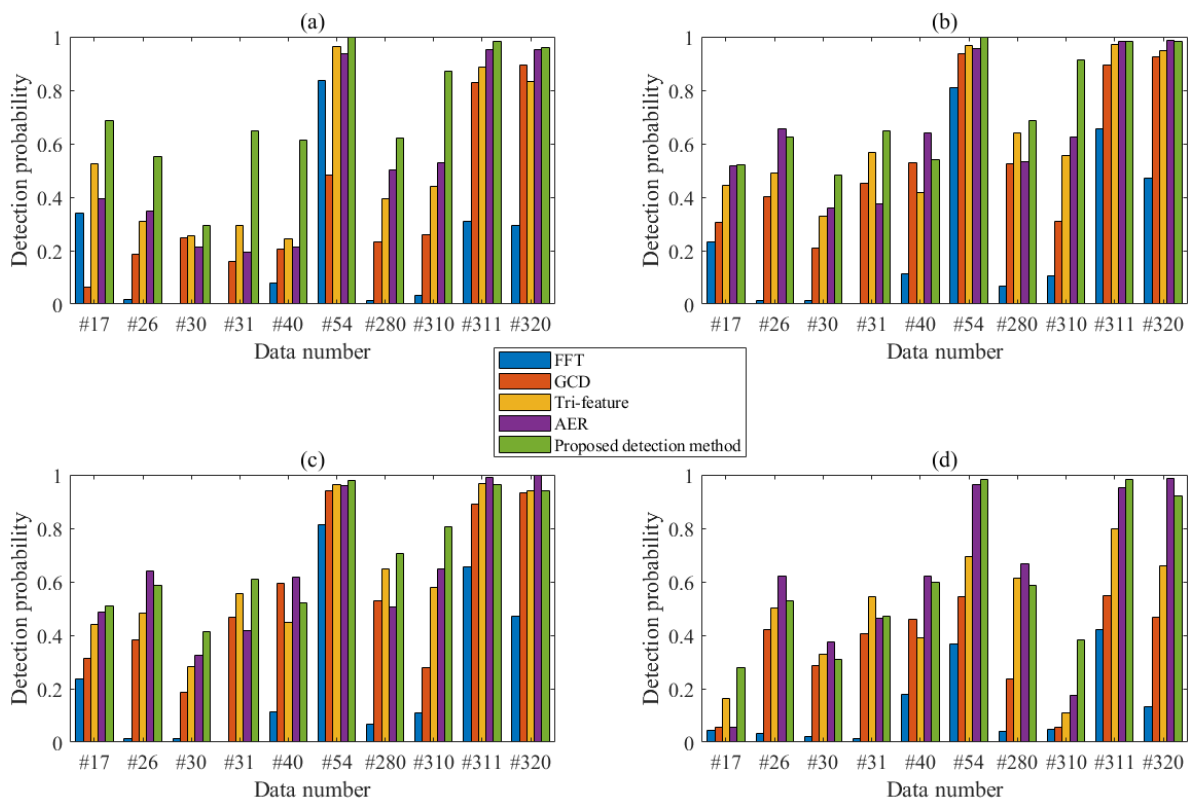


Figure 7. Contrasts of detection probabilities of five detection methods at (a) HH, (b) HV, (c) VH and (d) VV, when $N = 1024$ and $P_{fa} = 10^{-3}$.

5. Conclusions

This paper first performs STFT on the original data to generate a TF distribution spectrogram. FAST algorithm is used to extract the CFPs in the TF distribution spectrogram as the first feature ζ_1 . ζ_2 is calculated by ζ_1 . DBSCAN is used to divide clusters and count them as ζ_3 , which finally results in ζ_4 . In order to enhance the distinction between sea clutter and target returns, the four features are picked up. According to CFP energy sequencing from small to large, the first and the last one-eighth of the CFPs are removed, and re-statistics are performed. Then, feature normalization is performed and a four-dimensional feature space is constructed. XGBoost algorithm is used as the classifier, and GA is introduced to optimize the hyperparameters in XGBoost. The judgment threshold is updated in real time according to the prediction value output by XGBoost, which controls classifiers' false alarm rates.

A FAST-4F detection method is proposed and verified with IPIX dataset. The experimental results show that proposed detection method has excellent detection performance. Compared with several currently existing detection methods, when $N = 512$, the FAST-4F is superior to other detection methods, and its performance is improved by more than 7%. When $N = 1024$, the performance of proposed detection method is improved by 13.8%. In summary, the FAST four-feature detection method has a good detection performance, a simple model and a fast calculation, and therefore is ready to be applied to the small target detections on the sea surface.

The detection method proposed in this paper still has some limitations. For example, TFD spectrograms manifest different distribution characteristics at different polarizations. Later studies may focus on TFD improvements for smoother and clearer two-dimensional images. In addition, this paper adopts a manual set of parameters in each algorithm. There is great room for more adaptive methods to improve its practicability so as to achieve a clearer and generalization ability. This section is not mandatory but can be added to the manuscript if the discussion is unusually long or complex.

Author Contributions: [-20]Conceptualization, D.Z. and H.X.; methodology, H.X.; software, D.Z.; validation, H.W., H.Z., X.L. and H.L.; formal analysis, D.Z.; resources, D.Z.; data curation, D.Z.; writing—original draft preparation, D.Z.; writing—review and editing, H.X. All authors have read and agreed to the published version of the manuscript.

Funding: This work is supported by National Natural Science Foundation of China (Grant No. 62171228) and the National Key Research and Development Program of China (Grant No. 2021YFE0105500).

Institutional Review Board Statement: Not applicable.

Informed Consent Statement: Not applicable.

Data Availability Statement: The data were downloaded from the following website: <http://soma.ece.mcmaster.ca/ipix/index.html>. (accessed on 27 May 2021). The data were measured with the McMaster IPIX Radar, a fully coherent X-band radar, with advanced features such as dual transmit/receive polarization, frequency agility, and stare/surveillance mode.

Conflicts of Interest: The authors declare no conflict of interest.

References

1. Chen, J.J.; Huang, M.J.; Qiu, W.; Zhao, H.Z.; Fu, Q. A Novel Method for CFAR Detector with Bi-Thresholds in Sea Clutter. *Acta Electron. Sin.* **2011**, *39*, 2135–2141.
2. Zhou, W.; Xie, J.; Li, G.; Du, Y. Robust CFAR Detector with Weighted Amplitude Iteration in Nonhomogeneous Sea Clutter. *IEEE Trans. Aerosp. Electron. Syst.* **2017**, *53*, 1520–1535. [[CrossRef](#)]
3. Hu, J.; Tung, W.W.; Gao, J. Detection of Low Observable Targets within Sea Clutter by Structure Function Based Multifractal Analysis. *IEEE Trans. Antennas. Propag.* **2006**, *54*, 136–143. [[CrossRef](#)]
4. Luo, f.; Zhang, D.; Zhang, B. The Fractal Properties of Sea Clutter and Their Applications in Maritime Target Detection. *IEEE Trans. Geosci. Remote Sens. Lett.* **2013**, *10*, 1295–1299. [[CrossRef](#)]
5. Shi, Y.L.; Wang, L.; Yao, T.T. Orthogonal Projection Constant False Alarm Rate Algorithm in Fractional Domain for Small Surface Targets. *IET Signal Process.* **2022**, *16*, 975–991.
6. Haykin, S.; Xiao, B.L. Detection of Signals in Chaos. *Proc. IEEE* **1995**, *83*, 95–122. [[CrossRef](#)]
7. Lo, T.; Leung, H.; Litva, J.; Haykin, S. Fractal Characterization of Sea-Scattered Signals and Detection of Sea-Surface Targets. *Proc. IEEE* **1993**, *140*, 243–250.
8. Chen, X.; Guan, J.; Bao, Z.; He, Y. Detection and Extraction of Target with Micromotion in Spiky Sea Clutter via Short-Time Fractional Fourier Transform. *IEEE Trans. Geosci. Remote Sens.* **2014**, *52*, 1002–1018. [[CrossRef](#)]
9. Zuo, L.; Li, M.; Zhang, X.; Wang, Y.; Wu, Y. An Efficient Method for Detecting Slow-Moving Weak Targets in Sea Clutter Based on Time–Frequency Iteration Decomposition. *IEEE Trans. Geosci. Remote Sens.* **2013**, *51*, 3659–3672. [[CrossRef](#)]
10. Duan, G.X.; Wang, Y.H.; Zhang, Y.M.; Wu, S.Y.; Lv, L.T. A Network Model for Detecting Marine Floating Weak Targets Based on Multimodal Data Fusion of Radar Echoes. *Sensors* **2022**, *22*, 9163. [[CrossRef](#)]
11. Xu, C.; He, Z.S.; Liu, H.C.; Li, Y.D. Bayesian Track-Before-Detect Algorithm for Nonstationary Sea Clutter. *J. Syst. Eng. Electron.* **2022**, *32*, 1338–1344.
12. Shui, P.L.; Li, D.C.; Xu, S.W. Tri-Feature-Based Detection of Floating Small Targets in Sea Clutter. *IEEE Trans. Aerosp. Electron. Syst.* **2014**, *50*, 1416–1430. [[CrossRef](#)]

13. Shi, S.N.; Shui, P.L. Sea-Surface Floating Small Target Detection by One-Class Classifier in Time-Frequency Feature Space. *IEEE Trans. Geosci. Remote Sens.* **2018**, *56*, 6395–6411. [[CrossRef](#)]
14. Wagner, S.A. SAR ATR by a Combination of Convolutional Neural Network and Support Vector Machines. *IEEE Trans. Aerosp. Electron. Syst.* **2016**, *52*, 2861–2872. [[CrossRef](#)]
15. Yan, Y.; Xing, H.Y. Small Floating Target Detection Method Based on Chaotic Long Short-Term Memory Network. *J. Mar. Sci. Eng.* **2021**, *9*, 651. [[CrossRef](#)]
16. Pei, J.F.; Yang, Y.; Wu, Z.; Ma, Y.; Huo, W.; Zhang, Y.; Huang, Y.; Yang, J. A Sea Clutter Suppression Method Based on Machine Learning Approach for Marine Surveillance Radar. *IEEE J. Sel. Topics Appl. Earth Observ. Remote Sens.* **2022**, *15*, 3120–3130. [[CrossRef](#)]
17. Yan, K.; Bai, Y.; Wu, H.C.; Zhang, X. Robust Target Detection within Sea Clutter Based on Graphs. *IEEE Trans. Geosci. Remote Sens.* **2019**, *57*, 7093–7103. [[CrossRef](#)]
18. Shi, Y.L.; Yao, T.T.; Guo, Y.X. Floating Small Detection Based on Graph Connected Density in Sea Surface. *J. Electron. Inf. Technol.* **2021**, *43*, 3185–3192.
19. Shi, Y.L.; Liu, Z.P.; Zhang, X.L.; Gu, W.L. Feature Detection of Floating Small Target on the Sea Surface Based on EMD Energy Proportion. *J. Syst. Eng. Electron.* **2021**, *43*, 300–310.
20. Zhao, W.J.; Jin, M.L.; Cui, G.L.; Wang, Y.M. Eigenvalues-Based Detector Design for Radar Small Floating Target Detection in Sea Clutter. *IEEE Geosci. Remote Sens. Lett.* **2022**, *19*, 3509105. [[CrossRef](#)]
21. Yang, C.L.; Chen, Z.X.; Yang, C.Y. Sensor Classification Using Convolutional Neural Network by Encoding Multivariate time Series as Two-Dimensional Colored Images. *Sensors* **2020**, *20*, 168. [[CrossRef](#)] [[PubMed](#)]
22. Luo, S.E.; Luo, L.Y. Adaptive Detection of an Unknown FH Signal Based on Image Features. In Proceedings of the 2009 5th International Conference on Wireless Communications, Networking and Mobile Computing, Beijing, China, 24–26 September 2009; pp. 1–4.
23. Lampert, T.A.; O’Keefe, S.E. A Survey of Spectrogram Track Detection Algorithms. *Appl. Acoust.* **2010**, *71*, 87–100. [[CrossRef](#)]
24. Feng, S.; Hua, X.Q.; Zhu, X.Q. Matrix Information Geometry for Spectral-Based SPD Matrix Signal Detection with Dimensionality Reduction. *Entropy* **2020**, *22*, 914. [[CrossRef](#)] [[PubMed](#)]
25. Rosten, E.; Drummond, T. Fusing Points and Lines for High Performance Tracking. In Proceedings of the Tenth IEEE International Conference on Computer Vision (ICCV’05), Beijing, China, 17–21 October 2005; Volume 1, pp. 1505–1508.
26. Rosten, E.; Drummond, T. Machine Learning for High-Speed Corner Detection. In Proceedings of the European Conference on Computer Vision, Graz, Austria, 7 May 2006; Springer: Berlin/Heidelberg, Germany, 2006; pp. 430–443.
27. Li, W.J.; Jing, J.; Di, S. Finger Vein Recognition Algorithm Based on FAST Feature Extraction. *Opt. Precis. Eng.* **2020**, *28*, 507–514.
28. Ester, M.; Kriegel, H.P.; Sander, J.; Xu, X. A Density-Based Algorithm for Discovering Clusters in Large Spatial Data Sets with Noise. In Proceedings of the International Conference on Knowledge Discovery and Data Mining, Portland, OR, USA, 2 August 1996; pp. 226–231.
29. Vapnik, V.N. An Overview of Statistical Learning Theory. *IEEE Trans. Neural Netw.* **1999**, *10*, 988–999. [[CrossRef](#)]
30. Tibshirani, R. Regression Shrinkage and Selection via the Lasso: A Retrospective. *J. R. Stat. Soc. Ser. B Methodol.* **2011**, *73*, 273–282. [[CrossRef](#)]
31. Elith, J.; Leathwick, J.R.; Hastie, T. A Working Guide to Boosted Regression Trees. *J. Anim. Ecol.* **2008**, *77*, 802–813. [[CrossRef](#)]
32. Chen, T.; Guestrin, C. XGBoost: A Scalable Tree Boosting System. In Proceedings of the 22nd ACM SIGKDD International Conference Knowledge and Discovery Data Mining, New York, NY, USA, 13 August 2016; pp. 785–794.
33. Jiang, Y.; Tong, G.X.; Yin, H.N.; Xiong, N.X. A Pedestrian Detection Method Based on Genetic Algorithm for Optimize XGBoost Training Parameters. *IEEE Access* **2019**, *7*, 118310–118321. [[CrossRef](#)]
34. Xu, S.W.; Zheng, L.B.; Pu, J.; Shui, P.L. Sea-Surface Floating Small Target Detection Based on Polarization Features. *IEEE Geosci. Remote Sens. Lett.* **2018**, *15*, 1505–1509. [[CrossRef](#)]
35. Xu, S.W.; Zhu, J.A.; Jiang, J.Z.; Shui, P.L. Sea-Surface Floating Small Target Detection by Multifeature Detector Based on Isolation Forest. *IEEE J. Sel. Topics Appl. Earth Observ. Remote Sens.* **2021**, *14*, 704–715. [[CrossRef](#)]

Disclaimer/Publisher’s Note: The statements, opinions and data contained in all publications are solely those of the individual author(s) and contributor(s) and not of MDPI and/or the editor(s). MDPI and/or the editor(s) disclaim responsibility for any injury to people or property resulting from any ideas, methods, instructions or products referred to in the content.